Proceedings of the DIS'2004, Štrbské Pleso, Slovakia

RECENT RESULTS FROM H1

T. GREENSHAW
Oliver Lodge Laboratory, Liverpool University
Liverpool L69 7ZE, ENGLAND
E-mail: green@liv.ac.uk

A brief review is given of some of the recent measurements made by the H1 Collaboration in *ep* collisions at HERA. These include studies of proton structure, of the production of heavy flavours, of the hadronic final state in diffractive and non-diffractive scattering and searches for physics beyond the Standard Model. The first results obtained in the collisions of protons with polarised positrons following the HERA upgrade are also presented.

1 Introduction

The year leading up to the DIS Conference in Štrbské Pleso has seen both further analysis of HERA I e^+p and e^-p data, taken before the HERA high luminosity and polarisation upgrade, and the emergence of the first HERA II results, using e^+p data taken since the upgrade. This brief review provides an introduction to some of the measurements made by the H1 Collaboration in this period. Further results, and more detail on the topics discussed here, may be found in the accompanying articles in these Proceedings.

The apparatus used in the studies reported here is described in [1]. The right-handed cartesian coordinate system used has its origin at the nominal ep interaction vertex within the H1 detector. The z axis is in the direction of the outgoing proton beam, the y axis points vertically upwards and the x axis towards the centre of the HERA ring. Polar angles, θ, are measured with respect to the z axis. The region with $\theta < \frac{\pi}{2}$ is termed "forward" and that with $\theta > \frac{\pi}{2}$ "backward". Electrons and positrons are referred to generically as electrons, unless otherwise specified.

Many of the measurements discussed here are made in neutral current (NC) deep-inelastic scattering (DIS), in which the interacting electron and proton exchange a photon or a Z^0 boson. The cross section for positron-proton DIS may be written:

$$\frac{d^2\sigma_{NC}}{dx\,dQ^2} = 2\pi\alpha_{em}^2 \left(\frac{1}{Q^2}\right)^2 \frac{Y_+}{x}\tilde{\sigma}_{NC},$$

where Q^2 is the squared four-momentum transferred from the positron to the proton and x is the Bjorken scaling variable. The reduced cross section, $\tilde{\sigma}_{NC}$, contains helicity factors, the photon and Z^0 couplings to the quarks (the latter being significant only at high Q^2) and the structure functions $F_2(x,Q^2)$, $xF_3(x,Q^2)$ and $F_L(x,Q^2)$ which are related to the parton densities in the proton. The quantity $Y_+ = 1+(1-y)^2$ gives the helicity dependence of the electroweak interaction, where y expresses the energy loss of the electron. From measurements of the cross section, the quantity $\tilde{\sigma}_{NC}$ can be extracted, or the results may be expressed in terms of $F_2(x,Q^2)$, the proton structure function which dominates the reduced cross section in most of the HERA phase space. In the quark-parton model (QPM), the purely electromagnetic part of F_2 is related to the quark and anti-quark densities in the proton, q and $\bar{q}$, by $F_2^{em} = x\sum e_q^2(q+\bar{q})$, where the sum runs over the quark species q with electric charge e_q.

The cross section for charged current (CC) deep inelastic positron-proton scattering, in which a W boson is exchanged, can be written:

$$\frac{d^2\sigma_{CC}}{dx\,dQ^2} = (1+P_e)\,\frac{G_F^2}{2\pi x}\left(\frac{m_W^2}{m_W^2+Q^2}\right)^2 \tilde{\sigma}_{CC}.$$

Here, G_F is the Fermi coupling constant and the reduced cross section $\tilde{\sigma}_{CC}$ again contains helicity factors and structure functions. In this case, the dependence on the beam polarisation P_e (the ratio of the difference of the number of right-handed and left-handed electrons to their sum) is explicitly included, as this is visible with the polarised data sample available at the time of the Štrbské Pleso DIS conference.

2 Cross section measurements at high x and low Q^2

H1 measurements of the NC DIS cross-section cover the vast majority of the kinematic region accessible at HERA [2,3]. That is, values of Q^2 ranging up to about $5\times 10^4\,\mathrm{GeV}^2$ and of Bjorken-x in the approximate range $10^{-5} < x < 0.7$. In much of this kinematic region, a precision of 2 to 3% is achieved. There are, however, areas where direct measurements cannot easily be made. For example, the limited acceptance of the experiment's calorimeters at the smallest electron scattering angles, θ_e, implies that measurements cannot be made at $Q^2 \lesssim 1\,\mathrm{GeV}^2$. This region is of particular interest as it corresponds to the transition between DIS and photoproduction. Shifting the interaction vertex forward within the detector gives access to smaller θ_e: a shift of about 70 cm allows measurements to be made down to $Q^2 \sim 0.35\,\mathrm{GeV}^2$. Studies of such data have allowed cross section measurements to be made at low Q^2 and at low x [4,5]. The region of intermediate or high x values at this Q^2 could then be accessed by decreasing the proton or electron beam energies, but such data are as yet not available. An alternative is to exploit the reduced energy of electrons which interact with the proton after radiating an energetic photon. In contrast to earlier such studies [6], the analysis described here does not require the observation of the radiated photon. Instead, its presence is inferred from energy and longitudinal momentum conservation, as is described in [7]. In figure 1, the resulting measurements are shown together with the previous shifted vertex data, results obtained using QED Compton events, the measurements of the ZEUS Collaboration using their Beam Pipe Tagger (BPT) [8] and earlier results from fixed target experiments.

Interestingly, in the kinematic region of this measurement, $F_2(x,Q2)$ can still be described using the form $F_2(x,Q2) = c(Q2)\cdot x^{-\lambda(Q2)}$ [9] and is also well described by a parameterisation motivated by the assumption that proton structure is fractal in nature [10].

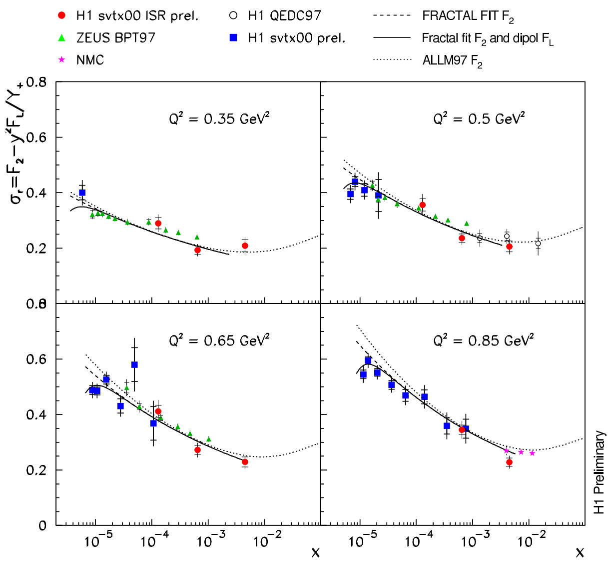

Figure 1. Reduced cross section measurements with $Q^2 < 1\,\mathrm{GeV}^2$ from H1, ZEUS and NMC.

3 Heavy flavour measurements

3.1 Contributions of charm and beauty to proton structure

Studies of the contribution of c and b quarks to proton structure allow the testing of perturbative QCD. In kinematic regions in which the mass m_Q of the heavy quarks is negligible, *e.g.* where $Q^2 >> m_Q^2$ as is the case here, the c and b quarks may be treated as forming part of the structure of the proton, just as do the flavours u, d and s. This approach is referred to as the zero mass variable flavour number scheme (ZM-VFNS) [11]. At values of $Q^2 \lesssim m_Q^2$, as in the measurement described in section 3.2, it is more appropriate to consider the heavy quarks as being produced via photon gluon fusion. This approach is referred to as the fixed flavour number scheme (FFNS) [12]. Reliable predictions over the entire kinematic range require the matching of the ZM-VFNS and FFNS regions, which has been carried out to order $\alpha_s(Q^2)$ [13] and to order $\alpha_s^2(Q^2)$ [14]. These approaches are referred to as variable flavour number schemes (VFNS).

In the analysis presented here, the H1 Central Silicon Tracker (CST) [15] is used to identify heavy quark events at $Q^2 > 110\,\mathrm{GeV}^2$ via the relatively long flight times of the particles into which these quarks hadronise. All tracks which are detected in the CST are investigated and those with the largest significance, *i.e.* the largest ratio of the transverse distance of closest approach (DCA) to the error in this quantity (σ_{DCA}), are used to measure the proportion of heavy flavours in the event sample. It is found that c events compose about 25% and b events about 3% of the cross section. The quantities $F_2^{c\bar{c}}$ and $F_2^{b\bar{b}}$, the contributions of charm and beauty to the proton structure function $F_2(x, Q^2)$, are evaluated and are shown in figure 2. ZM-VFNS, FFNS and VFNS based calculations are all able to provide a reasonable description of the data. This analysis, which provides the first ever measurement of the beauty content of the proton, is described in more detail in [16].

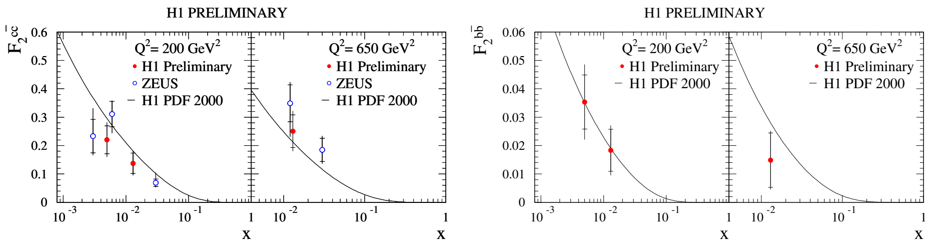

Figure 2. The contribution of charm $F_2^{c\bar{c}}$ (left) and beauty $F_2^{b\bar{b}}$ (right) to the proton structure function $F_2(x, Q^2)$.

3.2 Beauty cross section measurements in DIS and photoproduction

An alternative approach to the identification of beauty is used in measurements at lower Q^2. In DIS, events of the type $ep \to ej\mu X$ are sought, while in photoproduction $ep \to ejj\mu X$ events are used, where the j are jets. Beauty quarks are identified using the transverse momentum of the muon with respect to the jet within which it is found, p_T^μ, and the impact parameter of the muon, δ, again measured using the CST. As is described in [17], a two dimensional fit to the (p_T^μ, δ) distribution allows the extraction of the proportion of beauty events in the sample and hence the determination of the cross sections shown in figure 3. The data are compared with QCD predictions made using the massive scheme (FFNS in DIS). At the higher values of the scales Q^2 and p_T^μ shown here these calculations are quite convincing, at the lower values less so.

4 Studies of the hadronic final state

4.1 Evidence for the production of a narrow anti-charmed baryon state

Following recent measurements in which evidence for the production of strange pentaquark states was found in the decays $\Theta_s \to K^+ n$ and $\Theta_s \to K^0 p$ [18], H1 performed a search for charmed pentaquark states in DIS [19]. D^* meson candidates decaying via the chain $D^{*+} \to D^0 \pi_s^+ \to K^- \pi^+ \pi_s^+$ (addition of the charge conjugate channel is assumed implicitly throughout unless otherwise stated) are identified by forming the mass difference $\Delta M = M(K^- \pi^+ \pi_s^+) - M(K^+ \pi^+)$. As the Q value of the decay $D^{*+} \to D^0 \pi_s^+$ is small, the quantity ΔM can be accurately measured and the phase space available for combinatoric background is small. Hence, signal to background ratios of better than $1 : 1$ are achieved. These D^{*+} candidates are then combined with a further particle which, according to specific energy loss (dE/dx) measurements, has a reasonable likelihood of being an anti-proton. The resulting spectrum in the quantity $M(K^- \pi^+ \pi_s^+ \bar{p}) - M(K^- \pi^+ \pi_s^+) + M(D^*)_{PDG}$,

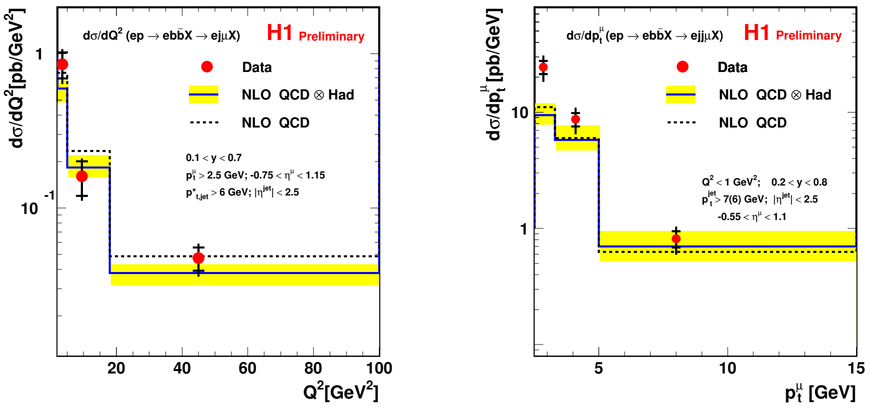

Figure 3. Differential cross section for the DIS process $ep \to ej\mu X$ (left) and for the photoproduction process $ep \to ejj\mu X$ (right) together with NLO QCD predictions at the parton level (dashed line) and the hadron level (solid line): the shaded band indicates the estimated uncertainties in the calculation due to renormalisation and other scale variations.

where $M(D^*)_{PDG}$ is the nominal D^* mass, is shown in figure 4. A clear peak is observed at 3.1 GeV, suggesting that there is a D^*p resonance at this mass, the quantum numbers of which make it a candidate for a charmed pentaquark state.

The background under the D^*p peak is well described by adding contributions from non-charmed events, obtained from the data by studying the spectrum resulting when the "wrong charge D^0" combination is taken in forming the D^{*+} *i.e.* $M(K^+\pi^+\pi_s^+) - M(K^+\pi^+)$, and from charmed events, obtained from Monte Carlo calculations. As is described in [19], the significance of this signal is determined to be greater than 5 Gaussian standard deviations. It is present in both charge conjugate decay channels and is also observed in an independent photoproduction sample.

4.2 The photoproduction of anti-deuterons

A further multi-quark state, of more conventional origin, is observed by H1 in photoproduction. Anti-deuterons are identified using specific energy loss measurements in the H1 Central Jet Chambers (CJCs) as described in [20]. The invariant cross section for anti-deuteron production, normalised to the total cross section, is found to be similar to that observed in central proton-proton collisions at the CERN ISR, but much lower than that in central gold-gold collisions at RHIC. In contrast to this, the ratio of the rate of anti-deuteron to anti-proton production in photoproduction at HERA is observed to be similar to that in both proton-proton and gold-gold collisions. These observations can be reconciled in the coalescence model for anti-deuteron production [21], if the size of the partonic "fireball" is much smaller in photoproduction and proton-proton interactions (at the point at which

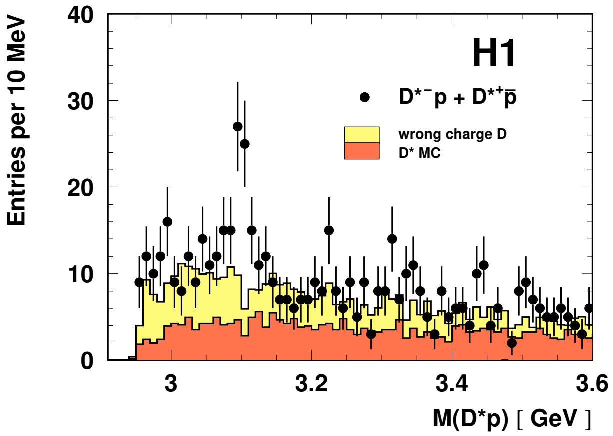

Figure 4. The D^*p mass spectrum compared with a two-component background model in which "wrong charge" combinations are used to describe non-charm related background and the "D^* MC" simulation describes background involving real D^* mesons.

the hadrons "freeze out") than is the case in heavy ion collisions [22].

It is interesting to note that anti-deuteron production has not been observed in e^+e^- annihilation in the $q\bar{q}$ continuum [23]: one may speculate that the photoproduction environment is more conducive to the production of complex "multi-quark" states than is that in e^+e^- annihilation.

No significant production of particles heavier than deuterons is observed in the H1 data and upper limits are set on the photoproduction cross sections for such particles.

4.3 Event shape studies

The study of the flow of hadronic energy and momentum, in terms of various event shape variables such as the thrust, T, provides a further means of testing QCD in DIS. The theoretical description of these infrared and collinear safe observables using fixed order calculations is problematic on two counts. Firstly, non-perturbative hadronisation effects can be large, even at perturbative scales. This can be addressed by using power corrections which are proportional to $1/Q$ [24]. These corrections introduce a free parameter, $\bar{\alpha}_0$, which must be determined from the measurements, but which is universal in the sense that it should have the same value for all event shape variables. Secondly, the convergence of the perturbative series at low values of the event shape variables is very poor, making a resummation to all orders in α_S necessary. Resummed next-to-leading logarithm (NLL) calculations, matched to NLO, have recently become available for many of the observables [25]. New H1 measurements are described here which take advantage of the larger data sample now available as well as using improved data reconstruction and correction techniques. Moreover, it is now possible to study the spectra of the event shape variables, not just their mean values as was done previously [26]. As is described in [27], additional event shape variables are also investigated which are sensitive to three jet production, and where resummed, matched calculations are near to completion.

Shown in figure 5 is the distribution of the variable $\tau = 1 - T$. The results of the fit from which α_s and $\bar{\alpha}_0$ are determined for this variable are also shown. Similar fits are performed for further "two jet" observables and the resulting pairs of values for α_s and $\bar{\alpha}_0$ are also shown in figure 5. The consistency of these pairs of values for the various observables has significantly improved when compared with previous measurements made using only the mean values of the variables and without the benefit of the improved calculations [26].

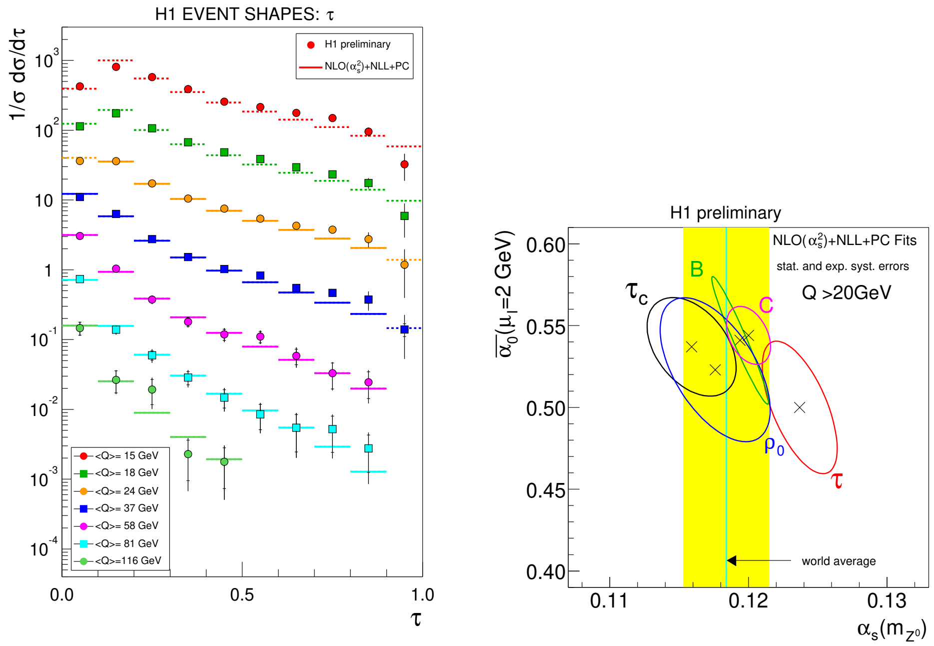

Figure 5. Left: Measured values of τ compared with the results of a fit based on NLO QCD including resummation and power corrections: the fit predictions are shown using dashed lines where the data points were not included in the fit. Right: the $1-\sigma$ contours in the $(\alpha_s, \bar{\alpha}_0)$ plane from fits to all the two jet event shape differential distributions studied.

4.4 Forward jet measurements

Many measurements of jet cross sections in DIS and photoproduction at HERA are successfully described by NLO QCD calculations. There are, however, phase space regions in which the description is not good. The measurements shown in figure 6 are a case in point. As is described in [28], these measurements show the cross section for the production in DIS of jets in the forward direction carrying a large proportion of the incoming proton's momentum. This region is studied as it is likely to expose the limitations of DGLAP [29] based calculations which resum terms $\sim \log Q^2$ but do not resum terms $\sim \log \frac{1}{x}$. At some small value of x, the latter must become significant and therefore DGLAP based calculations inappropriate. Indeed, the calculations shown in figure 6 lie below the data at small x, suggesting that in this kinematic regime the HERA data require that account be taken of large $\log \frac{1}{x}$ terms. This is done in calculations based on the BFKL [30] and CCFM [31] equations. The former resum terms $\sim \log \frac{1}{x}$ while the latter incorporate angular ordering effects and reproduce both the DGLAP and BFKL limits. However, as is discussed in [28], Monte Carlo calculations based on the CCFM equation [32] do not yet provide a good description of the data. The calculations require unintegrated parton distributions as input (*i.e.* distributions which include the k_T dependence) and the description of the forward jet data is observed to be sensitive to these. Further work is necessary to measure these unintegrated distributions; this will hopefully result in a better description of the forward jet data. Currently, the best representation of these measurements is provided by DGLAP based simulations [33] which allow the virtual photon to have structure. This is intuitively reasonable, as there are regions in which the partons from the proton may be considered to be probing the photon's structure as the jet transverse momentum, p_t, is larger than the photon's virtuality, Q. A reasonable description of the data in a large proportion of the investigated phase space is also provided by a Monte Carlo program [34] based on the colour dipole model [35].

4.5 Studies of the diffractive final state

H1 measurements of the structure of diffraction have been used to extract diffractive parton distributions using the DGLAP framework at NLO [36]. These measurements now cover the low Q^2 [37], intermediate Q^2 [36] and high Q^2 [38] regions: the entire phase space accessible with the data taken before the HERA upgrade. As has recently been demonstrated, diffractive cross sections factorize in DIS [39], hence this set of parton distributions should be applicable to all diffractive processes. This can be tested at HERA by investigating how well calculations using these distributions can describe the diffractive final state. Here, H1 measurements of jet and D^* production in diffraction, shown in figure 7, are compared with NLO QCD calculations [40]. The calculations are in agreement with the data within the remaining uncertainties. Data to be taken with the very forward proton spectrometer at H1 [41] will allow the uncertainties in these measurements to be reduced.

As is described in [43], H1 measurements of the final state in diffraction have recently been extended to cover the diffractive photoproduction of high p_T photons. The measurements are found to be in agreement with a perturbative QCD based model which uses the leading logarithm approximation of BFKL.

5 Physics beyond the Standard Model

5.1 General search for new phenomena

Most searches for physics beyond the Standard Model (SM) investigate a specific signature predicted by a particular new theory. The study described here is the

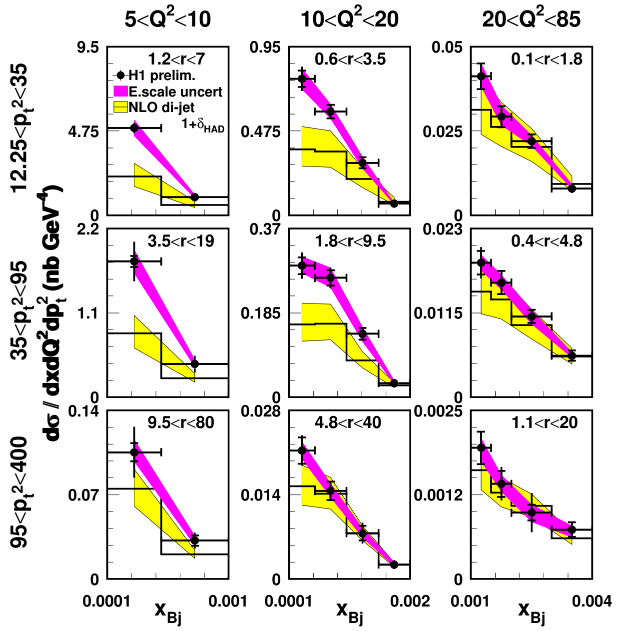

Figure 6. The triple differential cross section for forward jet production as a function of x, in bins of Q^2 and jet p_t^2. The band underneath the data points illustrates the experimental uncertainties due to the accuracy with which the calorimeter energy scale is known. The band underneath the NLO calculations illustrates the uncertainties arising from the choice of renormalisation scale. The coverage in $r = p_t^2/Q^2$ is shown in each bin.

first attempt at HERA to search for new physics in a model independent way. Event classes that are likely to reveal the presence of processes beyond the SM are identified and the rate at which they occur compared with SM predictions. Any excess is then a possible signature for new physics. The final states used in defining the event classes are all required to contain at least two entities with $p_T > 20\,\mathrm{GeV}$ in the polar angle range $10^\circ < \theta < 140^\circ$, *i.e.* isolated electrons, muons, jets, photons or neutrinos are sought, the latter being characterised by a missing transverse momentum ($\not{p}_T$) of more than 20 GeV. The measured rates of events containing these entities are compared with predictions based on a suite of Monte Carlo programs, as described in [44]. The results are shown in figure 8. The largest discrepancies between the data and the expectations are found to be in the event class containing a muon, a jet and $\not{p}_T$. An excess of events over SM expectations has previously been reported by H1 in this channel and in the channel in which the muon is replaced by an electron [45].

5.2 Studies of τ leptons

The excess of events containing isolated electrons or muons, significant hadronic transverse momentum, p_T^X, and $\not{p}_T$ motivated a search for similar events containing τ leptons. Algorithms for the identification of the “one prong” decays of τ leptons

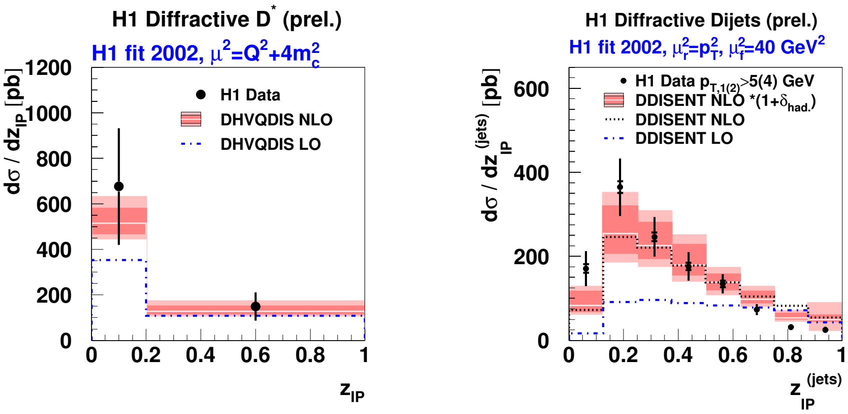

Figure 7. Left: Differential cross section for D^* meson production in diffractive DIS shown as a function of $z_{I\!P}$, an estimator for the longitudinal momentum fraction of the diffractive exchange entering the hard scattering process. Right: Differential cross section for dijet production in diffractive DIS from [42] corrected to the jet transverse momentum region $p_{T,1(2)} > 5(4)$ GeV.

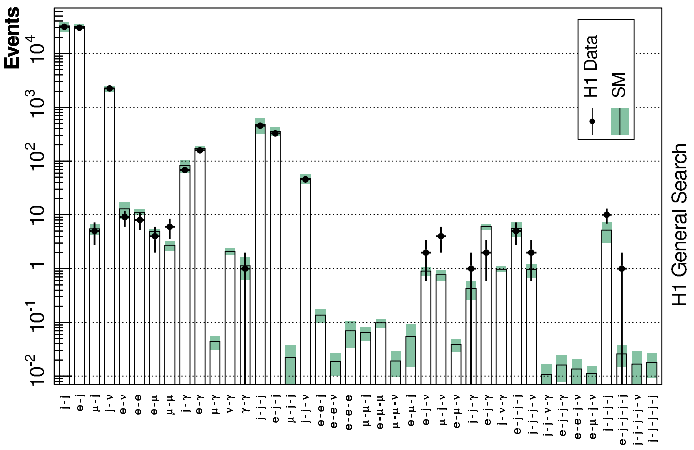

Figure 8. The data and the SM expectation for all event classes with a SM expectation greater than 0.01 events. The analysed data sample corresponds to an integrated luminosity of 117 pb^{-1}. The error bands on the predictions include model uncertainties and experimental systematic errors added in quadrature.

were developed and used to study the elastic τ pair production process $ep \to \tau\bar{\tau}p$. The rate of these events was found to match SM expectation, the dominant production mechanism being two-photon interactions. A search was then performed for isolated τ leptons associated with high p_T^X and $\not{p}_T$ [46]. No events were observed in the data taken prior to the HERA upgrade. The sensitivity in the τ channel is such that this result is compatible with both the SM expectation and the H1 observations of an excess of isolated muon and electron events.

5.3 Search for bosonic stop decays

One possible supersymmetric (SUSY) source of the isolated lepton events with large p_T^X and $\not{p}_T$ mentioned above is s-channel R-parity violating ($R\!\!\!/_p$) stop ($\tilde{t}$) production followed by the bosonic decay of the $\tilde{t}$, as is illustrated in figure 5.3. No evidence was found for either bosonic $\tilde{t}$ decays or direct $R\!\!\!/_p$ decays of the $\tilde{t}$, allowing the limits shown in figure 5.3 to be placed on the $\tilde{t}$ mass and the $R\!\!\!/_p$ coupling λ'_{131} [47]. This search complements previous studies of $R\!\!\!/_p$ SUSY performed by H1 [48,49].

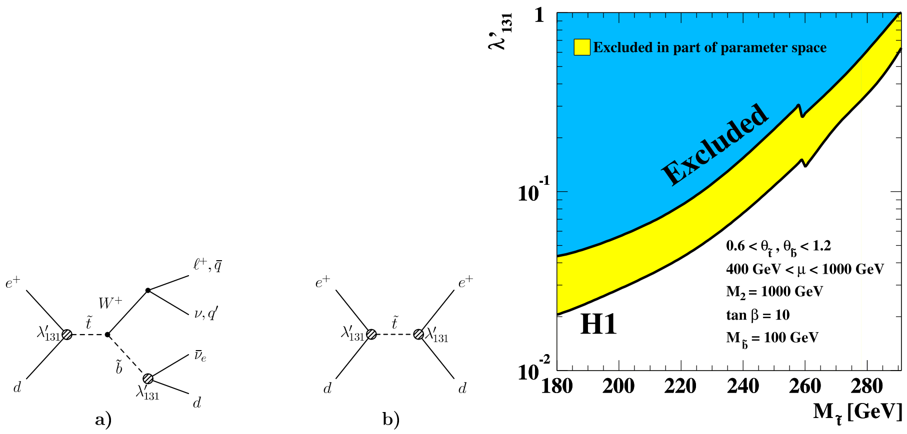

Figure 9. Left: Lowest order s-channel diagram for $R\!\!\!/_p\,\tilde{t}$ production at HERA followed by a) the bosonic decay of the $\tilde{t}$ and b) the $R\!\!\!/_p$ decay of the $\tilde{t}$. Right: Exclusion limits at the 95% CL on the $R\!\!\!/_p$ coupling λ'_{131} as a function of the $\tilde{t}$ mass for a sbottom mass $M_{\tilde{b}} = 100\,\mathrm{GeV}$. The limits are derived from a scan of the Minimal SUSY Standard Model parameter space $0.6 < \theta_{\tilde{b},\tilde{t}} < 1.2$, $400\,\mathrm{GeV} < \mu < 1000\,\mathrm{GeV}$, $M_2 = 1000\,\mathrm{GeV}$ and $\tan\beta = 10$. The two full curves indicate the regions excluded in all (dark) or part (light) of the parameter space investigated.

6 Physics at HERA II

6.1 Charged current cross section as a function of polarisation

The HERA upgrade provided not only an increase in the ep luminosity but also longitudinal polarisation of the electrons and positrons at the H1 and ZEUS interaction regions. At the time of this conference, slightly over $15\,\mathrm{pb}^{-1}$ of $e^+_R p$ data had been accumulated with a mean e^+ polarisation of about 30%. These data allowed a first measurement of the polarised CC DIS cross section to be made, as is described in [50]. The results are shown in figure 10 together with the CC cross section obtained in unpolarised CC interactions prior to the HERA upgrade and

H1 Preliminary

1994-2004 $e^{\pm}p$ $\mathcal{L} = 163\,\mathrm{pb}^{-1}$	Electron Obs./SM (% signal)	Muon Obs./SM (% signal)	Combined Obs./SM (% signal)
Full sample	18/15.4±2.1 (71%)	9/4.1±0.7 (86%)	27/19.5±2.8 (74%)
$P_T^X > 25$ GeV	8/2.6±0.5 (82%)	6/2.5±0.5 (88%)	14/5.1±1.0 (85%)

Table 1. Summary of the H1 results of searches for events with isolated electrons or muons and missing transverse momentum in the full HERA data set. Results are shown for the full data sample and for the sub-sample with $P_T^X > 25$ GeV. The number of observed events is compared to the SM prediction. The signal component of the SM expectation, dominated by real W production, is given as a percentage in parentheses. The quoted errors contain statistical and systematic uncertainties added in quadrature.

the expectations of the SM using the parton distribution functions determined by H1. The data are seen to be in good agreement with the expectations, confirming that the helicity structure of the charged current is as expected in the SM.

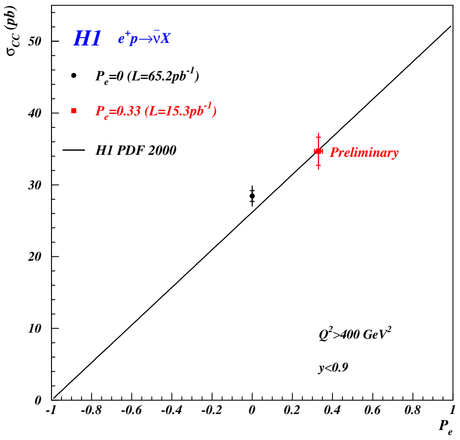

Figure 10. The dependence of the e^+p CC cross section on the positron beam polarisation P_e is shown. The data are compared to the prediction from the H1 PDF 2000 fit.

6.2 Searches for physics beyond the Standard Model at HERA II

Searches for new physics in the recent HERA data taken by H1 have concentrated on the areas in which anomalies have previously been observed, such as the events with isolated leptons, large p_T^X and $\not{p}_T$. The results of the searches for such events in all the HERA data available to date are shown in table 1.

Isolated lepton events continue to appear in the HERA II data at a rate compatible with the expectations from the HERA I measurements and somewhat above that expected from the SM.

7 Summary

Continued analysis of the H1 data taken before the HERA luminosity and polarisation upgrade has produced many new results, for example the first ever measurement of the contribution of b quarks to proton structure, first measurements of event shape distributions in DIS, the first observation of a charmed pentaquark state and improved measurements of proton structure in the extremes of the kinematic plane accessible at HERA. Measurements have now also been made using the data obtained since the HERA upgrade. The determination of the helicity dependence of charged current deep-inelastic positron-proton scattering is a highlight of this new period of HERA running, as is the fact that H1 continues to see a higher rate of isolated lepton events with large missing transverse momentum than expected in the Standard Model. Understanding these and other measurements will require large amounts of positron-proton and electron-proton data, which will also allow further extension of the range over which the structure functions of the proton are precisely measured. Obtaining large data samples is not the only option for future HERA operation however; significant improvements in the determination of the contribution of the gluon to proton structure, with concomitant improvements in the precision of the measurement of the strong coupling constant, can be obtained if HERA runs at reduced proton beam energy. In summary, with HERA now delivering the highest luminosities it has yet achieved, a rich harvest of new results can be expected at the next DIS workshop in Madison, Wisconsin and in the years to come.

Acknowledgements

I thank all of my H1 colleagues for their hard work, enterprise and enthusiasm, which has resulted in the production of the measurements discussed here and has made and continues to make H1 a most pleasant place to work. It is also a pleasure to thank our hosts in Štrbské Pleso, who did a truly excellent job of organising the DIS 2004 workshop and fostering an atmosphere in which lively discussion thrived. Finally, I thank Max Klein for carefully checking through this manuscript.

References

1. I. Abt *et al.* [H1 Collaboration], Nucl. Inst. Meth. **A386** (1997) 310 and 348.
2. C. Adloff *et al.* [H1 Collaboration], Eur. Phys. J. **C19** (2001) 269.
3. C. Adloff *et al.* [H1 Collaboration], Eur. Phys. J. **C30** (2003) 1.
4. C. Adloff *et al.* [H1 Collaboration], Nucl. Phys. **B497** (1997) 3.
5. H1 Collaboration, contributed paper 082 to EPS03, Aachen.
6. H1 Collaboration, contributed paper 976 to ICHEP02, Amsterdam.
7. A. Petrukhin [H1 Collaboration], these Proceedings.
8. J. Breitweg *et al.* [ZEUS Collaboration], Phys. Lett. **B487** (2000) 53.
9. C. Adloff *et al.* [H1 Collaboration], Phys. Lett. **B520** (2001) 183.
10. T. Lastovicka, Eur. Phys. J. **C24** (2002) 529.
11. H.L. Lai *et al.* Phys. Rev. **D55** (1997) 1280;

A.D. Martin, W.J. Stirling and R.G Roberts, Phys. Rev. **D50** (1994) 6734.

12. E. Laenen, S. Riemersma, J. Smith and W.L van Neerven, Nucl. Phys. **B392** (1993) 162;
 E. Laenen, S. Riemersma, J. Smith and W.L van Neerven, Nucl. Phys. **B392** (1993) 229;
 S. Riemersma, J. Smith and W.L van Neerven, Phys. Lett. **B347** (1995) 143.
13. F.I. Olness and W.K. Tung, Nucl. Phys. **B308** (1988) 813;
 M.A.G. Aivazis, J.C. Collins, F.I. Olness and W.K. Tung, Phys. Rev. **D50** (1994) 3102;
 M.A.G. Aivazis, F.I. Olness and W.K. Tung, Phys. Rev. **D50** (1994) 3085;
 M. Kramer, F.I. Olness and D.E. Soper, Phys. Rev. **D62** (2000) 096007;
 S. Kretzer, H.L. Lai, F.I. Olness and W.K. Tung, hep-ph/0307022;
 R.S. Thorne and R.G. Roberts, Phys. Rev. **D57** (1998) 6871;
 R.S. Thorne and R.G. Roberts, Phys. Lett. **B421** (1998) 303;
 R.S. Thorne and R.G. Roberts, Eur. Phys. J. **C19** (2001) 339;
 M. Cacciari, M. Greco and P. Nason, JHEP **9805** (1998) 007;
 M. Cacciari, S. Frixione and P. Nason, JHEP **0103** (2001) 006.
14. M. Buza, Y. Matiounine, J. Smith and W.L. van Neerven, Phys. Lett. **B411** (1997) 211;
 A. Chuvakin, J. Smith and W.L. van Neerven, Phys. Rev. **D61** (2000) 096004;
 A. Chuvakin, J. Smith and W.L. van Neerven, Phys. Rev. **D62** (2000) 036004.
15. D. Pitzl *et al.* Nucl. Inst. Meth. **A454** (2000) 334.
16. P.D. Thompson [H1 Collaboration], these Proceedings.
17. A.B. Meyer [H1 Collaboration], these Proceedings.
18. T. Nakano *et al.* [LEPS Collaboration], Phys. Rev. Lett. **91** (2003) 012002;
 J. Barth *et al.* [SAPHIR Collaboration], Phys. Lett. **B572** (2003) 127;
 V. Kubarovsky *et al.* [CLAS Collaboration], Phys. Rev. Lett. **91** (2003) 252001;
 V. Kubarovsky *et al.* [CLAS Collaboration], Phys. Rev. Lett. **92** (2004) 032001; erratum, ibid. 049902.
19. A. Aktas *et al.* [H1 Collaboration], Phys. Lett. **B588** (2004) 17.
20. A. Aktas *et al.* [H1 Collaboration], Eur. Phys. J. **C36** (2004) 413.
21. S.T. Butler and C.A. Pearson, Phys. Rev. **129** (1963) 836;
 A. Schwarzschild and C. Zupancic, Phys. Rev. **129** (1963) 854;
 H.H. Gutbrod *et al.* Phys. Rev. Lett. **37** (1976) 667;
 H. Sato and K. Yazaki, Phys. Lett. **B98** (1981) 153;
 L.P. Csernai and J.I. Kapusta, Phys. Rep. **131** (1985) 223.
22. R. Scheibl and U. Heinz, Phys. Rev. **C59** (1999) 1585;
 A. Polleri, R. Mattiello, I.N. Mishustin and J.P. Bondorf, Phys. Lett. **B473** (2000) 193.
23. H. Albrecht *et al.* [ARGUS Collaboration], Phys. Lett. **B236** (1990) 102;
 R. Akers *et al.* [OPAL Collaboration], Z. Phys. **C67** (1995) 203.
24. Y.L. Dokshitzer and B.R. Webber, Phys. Lett. **B404** (1997) 321.
25. M. Dasgupta and G.P. Salam, JHEP **0208** (2002) 032.
26. C. Adloff *et al.* [H1 Collaboration], Phys. Lett. **B406** (1997) 256;
 C. Adloff *et al.* [H1 Collaboration], Eur. Phys. J. **C14** (2000) 255; erratum ibid. **C18** (2000) 417.

27. W. Yan [H1 Collaboration], these Proceedings.
28. A. Knutsson [H1 Collaboration], these Proceedings.
29. V. Gribov and L. Lipatov, Sov. J. Nucl. Phys. **15** (1972) 438 and 675;
L. Lipatov, Sov. J. Nucl. Phys. **20** (1975) 94;
G. Altarelli and G. Parisi, Nucl. Phys. **B126** (1977) 298;
Y. Dokshitzer, Sov. Phys. JETP **46** (1977) 641.
30. E. Kuraev, L. Lipatov and V. Fadin, Sov. Phys. JETP **44** (1976) 443;
E. Kuraev, L. Lipatov and V. Fadin, Sov. Phys. JETP **45** (1977) 199;
Y. Balinsky and L. Lipatov, Sov. J. Nucl. Phys. **28** (1978) 822.
31. M. Ciafaloni, Nucl. Phys. **B296** (1988) 49;
S. Catani, F. Fiorani and G. Marchesini, Phys. Lett. **B234** (1990) 339;
S. Catani, F. Fiorani and G. Marchesini, Nucl. Phys. **B336** (1990) 18;
G. Marchesini, Nucl. Phys. **B445** (1995) 49.
32. H. Jung and G. Salam, Eur. Phys. J. **C19** (2001) 351;
H. Jung, Comp. Phys. Comm. **143** (2002) 100.
33. H. Jung, Comp. Phys. Comm. **86** (1995) 147.
34. L. Lönnblad, Comp. Phys. Comm. **71** (1992) 15;
L. Lönnblad, Zeit. Phys. **C65** (1995) 285.
35. G. Gustafson, Phys. Lett. **B175** (1986) 453;
G. Gustafson and U. Pettersson Nucl. Phys. **C306** (1988) 746.
36. H1 Collaboration, paper 980 submitted to EPS 2003, Aachen.
37. H1 Collaboration, paper 981 submitted to ICHEP 2002, Amsterdam.
38. H1 Collaboration, paper 090 submitted to EPS 2003, Aachen.
39. J. Collins, Phys. Rev. **D57** (1998) 3051; erratum, ibid. **D61** (2000) 019902.
40. S. Schätzel [H1 Collaboration], these Proceedings.
41. L. Favart, Proc. DIS 2000, Liverpool, England, Ed.s J.A. Garvey and T. Greenshaw, p. 618.
42. C. Adloff it et al. [H1 Collaboration] Eur. Phys. J. **C20** (2001) 29.
43. J. Olsson [H1 Collaboration], these Proceedings.
44. M. Peez [H1 Collaboration], these Proceedings.
45. V. Andreev *et al.* [H1 Collaboration], Phys. Lett. **B561** (2003) 241.
46. G. Brandt [H1 Collaboration], these Proceedings.
47. A. Vest [H1 Collaboration], these Proceedings.
48. C. Adloff *et al.* [H1 Collaboration], Eur. Phys. J. **C20** (2001) 639.
49. A. Aktas *et al.* [H1 Collaboration], Eur. Phys. J. **C36** (2004) 425.
50. O. Henshaw [H1 Collaboration], these Proceedings.